Raman microscopy and infrared optical properties of SiGe Mie resonators formed on SiO 2 via Ge condensation and solid state dewetting

Vladimir Poborchii, Mohammed Bouabdellaoui, Noriyuki Uchida, Antoine Ronda, Isabelle Berbezier, Thomas David, Carmen Ruiz, Mimoun Zazoui, Robert Paria Sena, Marco Abbarchi, et al.

Raman microscopy and infrared optical properties of SiGe Mie resonators formed on SiO_2 via Ge condensation and solid state dewetting

Vladimir Poborchii,[1] Mohammed Bouabdellaoui,[2,3] Noriyuki Uchida,[1] Antoine Ronda,[2] Isabelle Berbezier,[2] Thomas David,[2] Carmen M. Ruiz,[2] Mimoun Zazoui,[3] Robert Paria Sena,[2] Marco Abbarchi,[2] and Luc Favre[2]

[1]*Nanoelectronics Research Institute, National Institute of Advanced Industrial Science and Technology, 1-1-1 Higashi, AIST Central-5, Tsukuba 305-8565, Japan*

[2]*Aix Marseille Univ, Université de Toulon, CNRS, IM2NP, Marseille, France*

[3]*Laboratory of Physics of Condensed Matter and Renewable Energy, Faculty of Sciences and Technology, Hassan II University of Casablanca, 146 Mohammedia, Morocco*

(Dated: December 16, 2019)

All-dielectric photonics is a promptly developing field of optics and material science. The main interest at visible and near-infrared frequencies is light management using high-refractive-index Mie-resonant dielectric particles. Most work in this area of research was done exploiting Si-based particles. Here, we study monocrystalline Mie-resonant particles made of Ge-rich SiGe alloys with refractive index higher than that of Si. These islands are formed via solid state dewetting of SiGe flat layers by using two different processes: i) dewetting of monocrystalline SiGe layers (60-80% Ge content) obtained via Ge condensation of SiGe on silicon on insulator, ii) dewetting of a SiGe layer deposited via molecular beam epitaxy on silicon on insulator and ex-situ Ge condensation, forming a Ge-rich shell surrounding a SiGe-core. Using high-spatial-resolution Raman microscopy we monitor Ge content x and strain ϵ of flat layers and SiGe-islands. We observe strain relaxation associated with formation of trading dislocations in the SiGe islands compared to the starting SiGe layers, as confirmed by TEM images. For initial high Ge concentration in the flat layers, the corresponding Ge content in the dewetted islands is lower, owing to diffusion of Si atoms from Si or SiO_2 into SiGe islands. The Ge content also varies from particle to particle on the same sample. Size and shape of the dewetted particles depend on the fabrication process: thicker initial SiGe layers lead to larger particles. Samples with narrow island size distribution display rather sharp Mie resonances in the 1000-2500 nm spectral range. Larger islands display Mie resonances at longer wavelength. Positions of the resonances are in agreement with the theoretical calculations in the discrete dipole approximation.

Corresponding author:
Marco Abbarchi (marco.abbarchi@im2np.fr)
Vladimir Poborchii (vladimir.poborchii@gmail.com)

I. INTRODUCTION

High-refractive-index sub-micrometric particles display strong electric and magnetic Mie resonances in their optical spectra. The resonant wavelength depends, among other parameters, on the size and shape of the particles. In contrast to metal particles displaying plasmonic resonances, the dielectric counterpart provides reduced light losses at visible and near-infrared frequencies. Thus, engineering all-dielectric optical metasurfaces consisting of such particles attracted much attention in the last decade[1–10]. In most of works, silicon was used as a building material for such structures due to relatively high refractive index n $\sim$ 3.4-3.5 in the infra-red (IR) spectral range and well-developed technology of Si nanostructure fabrication. Less explored is the case of SiGe-based particles that provides a better light confinement thanks to its larger refractive index at IR frequencies (for Ge n $\sim$ 4).

Compared to relatively expensive nano-fabrication methods for optical metasurfaces, such as e-beam or nano-imprint lithography and reactive ion etching that involve many fabrication steps, a dewetting technique based only on annealing of a thin silicon layer on SiO_2 (ultra-thin silicon on insulator, UT-SOI) looks attractive due to its ease of implementation and wafer-scale character[11–17]. In addition, the use of dewetting allows for the fabrication of defect-free, monocrystalline particles having atomically smooth facets.

The advantages offered by dewetting go beyond most common self-assembly methods for 3D structures made of semiconductors. In fact, these methods usually rely on Stranski Krastanov growth for strained III-V and IV-IV 3D heterostructures[18] and droplet epitaxy[19] (only for III-V). These approaches demand for an epitaxial relation between the material composing the 3D structures and the underlying (crystalline) substrate. Solid state dewetting can produce a plethora of different structures on (amorphous) SiO_2 providing an electrically insulating barrier for the 3D nano-achitectures, that is a straightforward advantage for the fabrication of electronic devices. Most importantly, for the implementation of dielectric metasurfaces, the presence of a non-absorbing, transparent, low-refractive index substrate, enables the formation of high quality-factor Mie modes[14,15] similar to those found for top-down fabrication[20].

A drawback of dewetting using commercial wafers, is the limited set of available specifications of UT-SOI (e.g. device thickness) and the high costs of Ge-rich layers (ultra-thin silicon-germanium on insulator, UT-SGOI). This limits the possibility to finely tune the main structural parameters of Mie resonators obtained with this self-assembly method such as their size, density, shape, composition and composition profile. In order to overcome these limitations, the deposition of silicon-germanium after[16] or during[17,21,22] dewetting allowed changing the particles size, shape and density, providing a versatile tool for engineering their optical properties.

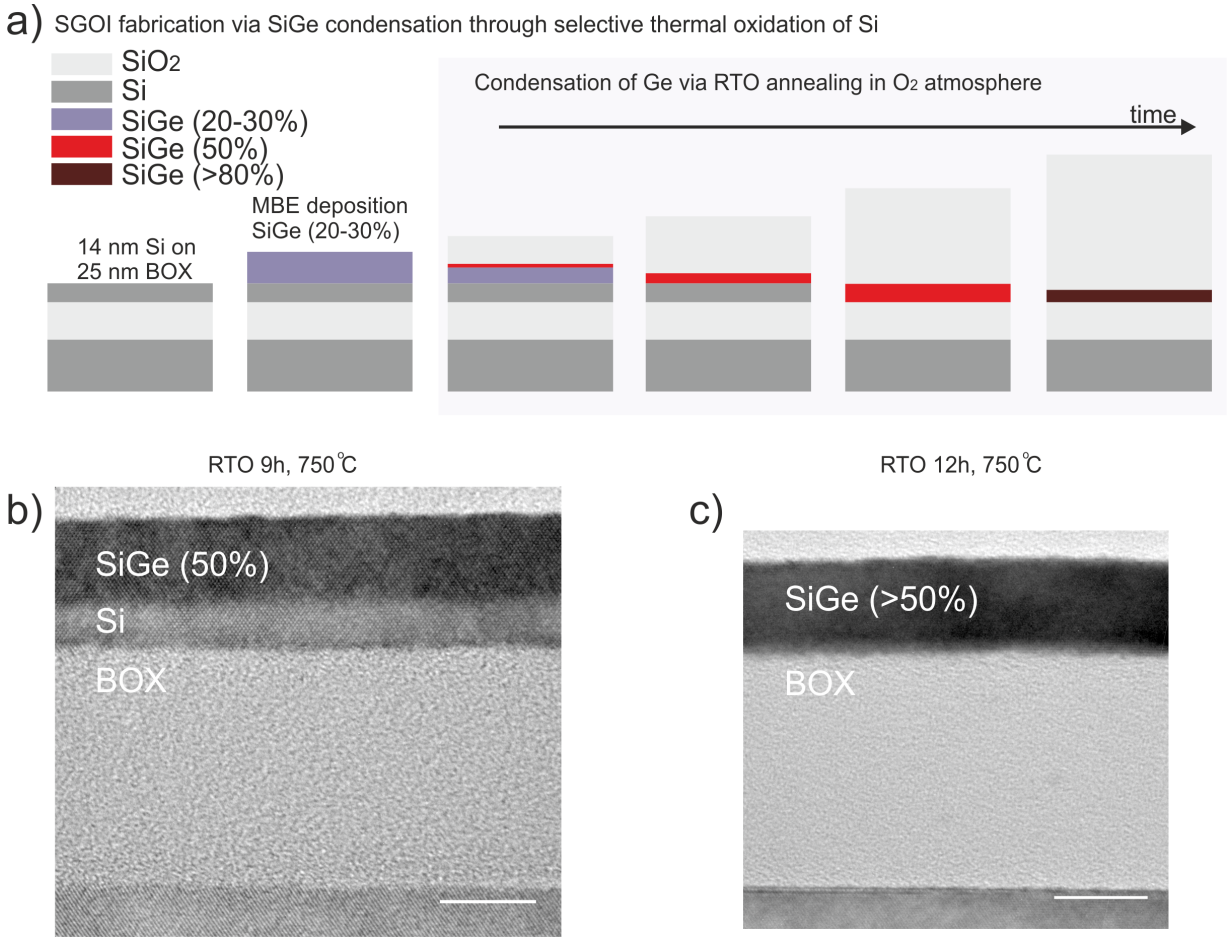

FIG. 1. a) Scheme of the SiGe alloys deposition on UT-SOI in the molecular beam reactor (MBE, first and second panel from the left) and of the (*ex-situ*) Ge condensation process in the rapid thermal oxidation (RTO third to fourth panel). b) Transmission electron microscopy (TEM) image of an initial 21 nm thick SiGe layer (22% Ge content) deposited on 14 nm UT-SOI and condensed for 9 hours in the RTO at 750°C. c) Same as b) for 12 hours condensation. Scales bar correspond to 10 nm.

Anti-reflection coatings, light-trapping effects in IR spectral range[17,23] and protein sensing[24] were recently demonstrated. In addition to this, exploiting a Ge-condensation process[16], Ge-rich shell can be formed around a Si-rich core, allowing to tune the composition profile and eventually the strain in the islands.

Here, we further develop this fabrication method showing the controlled formation of SiGe islands from monocrystalline layers (UT-SGOI) obtained by combining: i) SiGe deposition on UT-SOI via molecular beam epitaxy, ii) *ex-situ* Ge-condensation of the flat layers via rapid thermal oxidation after molecular beam epitaxy deposition, allowing a fine tuning of Ge composition and iii) Ge condensation after dewetting, forming a Ge-rich shell around the islands. By high-spatial resolution Raman microscopy we monitor the SiGe islands obtained by a variety of dewetting and Ge-condensation techniques, studying their strain and composition with respect to the starting flat structures. Finally, we demonstrate Mie resonances in IR spectra of SiGe islands and their tuning depending on the fabrication process.

II. EXPERIMENTAL

One set of UT-SGOI substrates was obtained by following a well-established procedure[25–28]. In Fig. 1 a), from the left to the right panel, the different steps are described: starting from a commercial UT-SOI substrate (14 nm of Si atop 25 nm of buried oxide, BOX), SiGe layers with variable thickness and Ge content were grown in a molecular beam epitaxy reactor. Some of these samples are then transferred in a rapid thermal oxidation oven where they are heated at high temperature in O_2 atmosphere. Depending on the annealing time and temperature, the thickness and Ge content of the final layers samples can be finely tuned providing, for example $Si_{1-x}Ge_x$ (x $\sim$ 0.5) on Si on the BOX or directly high Ge content (x 0.5) UT-SGOI as deduced by transmission electron microscopy (TEM) characterization (Fig. 1 b) and c), performed with a JEOL 3000 kV).

In order to dewet the condensed layers, the UT-SGOI was further processed by removing the top SiO_2 via wet, chemical etching (HF 4% for 5 minutes). The condensed layers

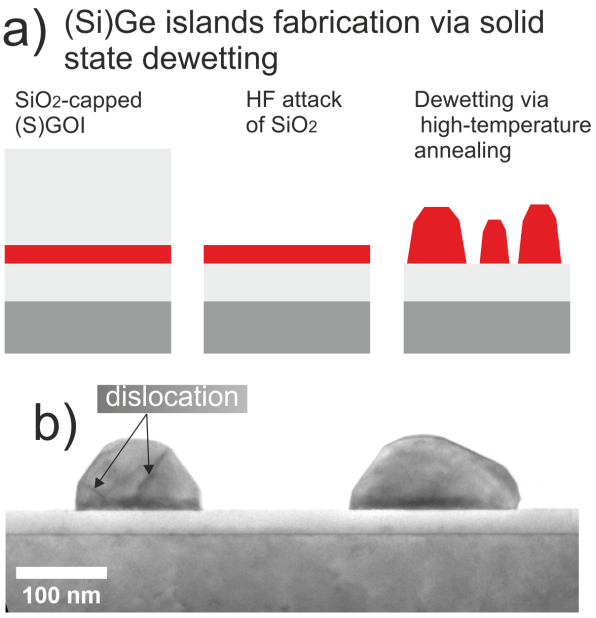

FIG. 2. a) Scheme of the chemical process for removing the capping SiO_2 obtained from the selective Si oxidation on top of the UT-SGOI (left and central panel) and dewetting in the MBE (right panel). b) Transmission electron micrograph of SiGe islands obtained by dewetting (800°C for 4 hours) an initial layer of 9.2 nm of SiGe (Ge content 50%) on Si 6 nm, as in Fig. 1 b). The arrow highlight the presence of dislocations.

were transferred in the molecular beam epitaxy reactor for high-temperature annealing, thus transforming the flat layers in SiGe islands20 (Fig. 2)[16]. Depending on the starting conditions of the 2D layers before dewetting (e.g. SiGe layer thickness deposited via molecular beam epitaxy, Ge content and SiGe thickness set by the rapid thermal oxidation process), we obtain islands with tunable average size and Ge content.

From TEM images of dewetted SiGe islands (Fig. 2 (c)) we can highlight the presence of dislocations springing from the interface between the residual pristine UT-SOI and the top SiGe island. This latter feature is not observed before dewetting in the flat layers. The Raman analysis (see later) confirms that, differently from the initial flat layers, the island are relaxed.

A last set SiGe islands was obtained via molecular beam epitaxy growth of 50 nm thick SiGe layers ($x \sim 0.3$) on 14 nm thick UT-SOI, *in-situ* dewetting and *ex situ* condensation in the rapid thermal oxidation oven, thus forming a Ge shell around a Si-rich core (Fig. 3), as described in Ref.[16]. From the SEM images of the islands after rapid thermal oxidation processing we can roughly estimate of a $\sim$100 nm thick SiO_2 shell around a 50 nm Ge-rich SiGe shell surrounding the Si-rich core in line with previous observations in similar samples. A more precise characterization of this kind of samples is obtained via high resolution transmission electron microscopy (Fig. 3 c)). 2D Fourier transform of high resolution TEM images accounts for the monocrystalline character of the lattice, as the hexagonal spot patterns observed in different parts of

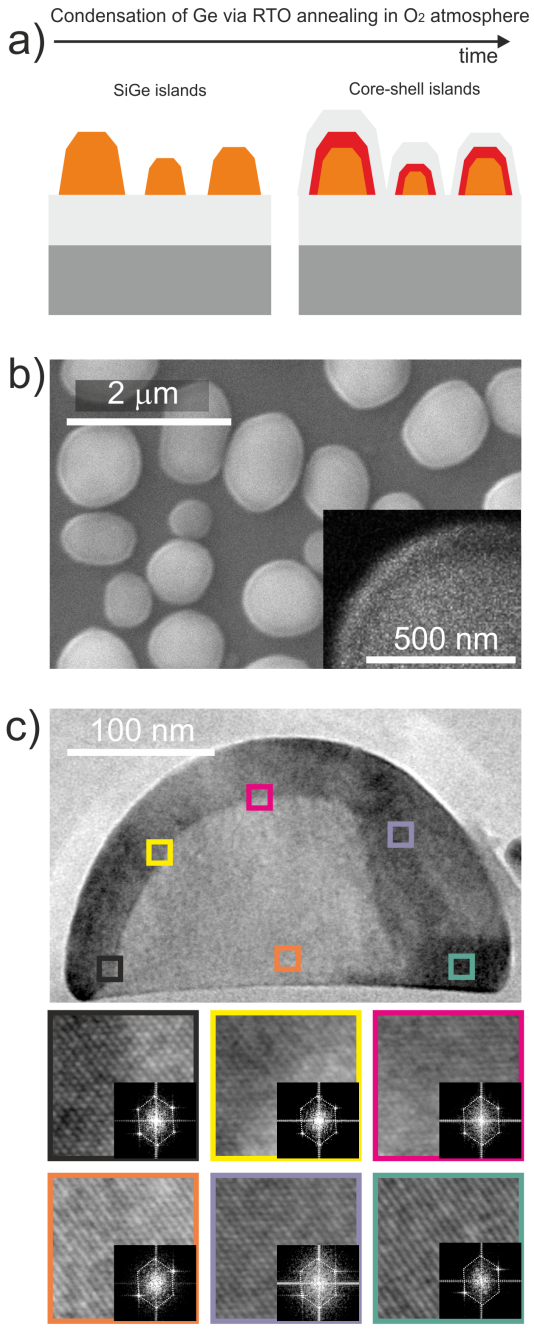

FIG. 3. a) Scheme of the Ge condensation process to form a Ge-rich shell surrounding the SiGe islands. b) Scanning electron microscope (SEM) image of the SiGe islands after condensation. The bottom right inset shows a blow up of an island highlighting the presence of a shell. c) High resolution transmission electron microscopy (TEM) of a SiGe island after condensation. The bottom panels show blow-ups of 6 selected areas of the islands core and the interface between core and shell. For each of them the 2D Fourier transform is provided as bottom-right inset. The asymmetric shape of the Ge-rich shell (dark part) surrounding the Si-rich core (light part) may depend on the misorientation of the TEM lamella with respect to the in-plane symmetry axes of the island.

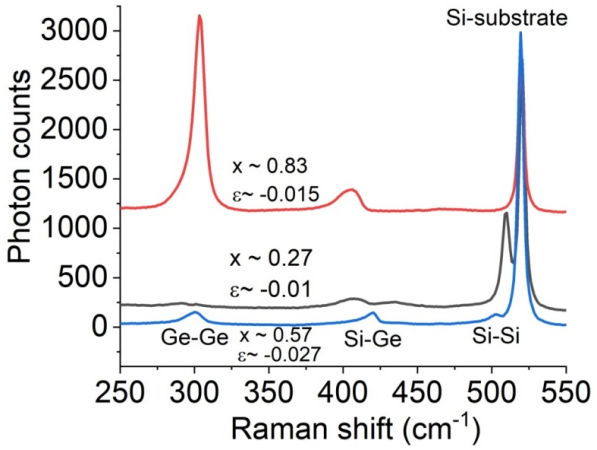

FIG. 4. Raman spectra of UT-SGOI substrates with different Ge content x. The Ge content x and strain ϵ determined from the Raman peak positions are displayed for each case. Black curve: 200 nm SiGe layer on 14 nm thick UT-SOI. Red curve: 9 nm SiGe on BOX. Blue curve: 9.2 nm SiGe on top of 6 nm Si.

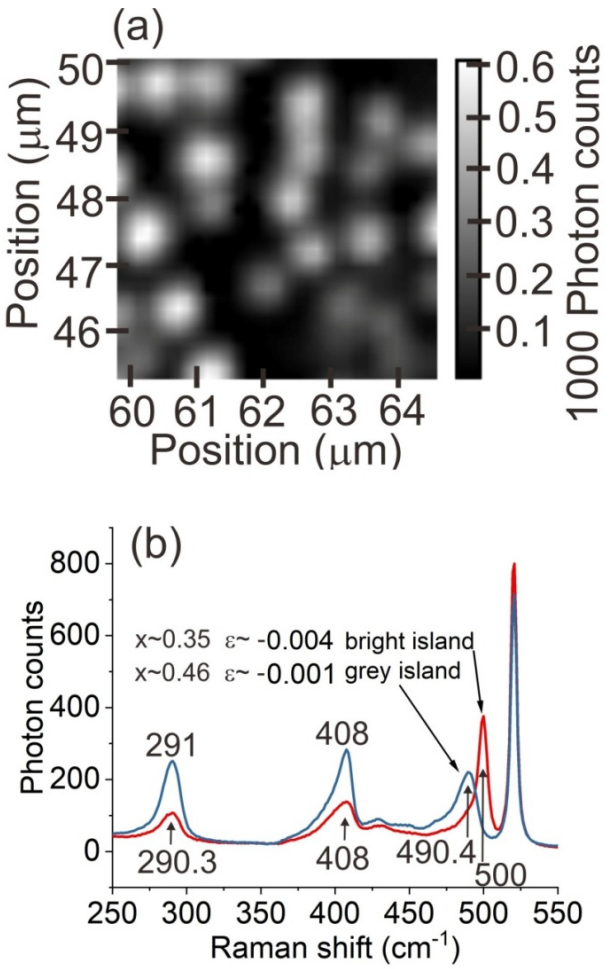

FIG. 5. (a) Raman intensity map of the Si-Si mode for the SiGe island sample fabricated from 9.2 nm thick SiGe layer on 6 nm thick Si with initial x $\sim$ 0.57; (b) Raman spectra of a bright SiGe island in the center of the Raman map (red curve) and of the dark grey island in the right-bottom part of the map (blue curve). The Ge content x and strain ϵ determined from the Raman peak positions are shown for each spectrum.

the island coincide within the experimental error.

Raman measurements were performed with Nanofinder-30 Raman/AFM system (Tokyo Instruments) equipped with a scanner allowing Raman mapping of a few-micron-size areas with $\sim$100 nm steps[13,29–33]. A 561 nm wavelength laser beam was focused by a 100$\times$ 0.95-numerical-aperture lens providing a $\sim$350 nm lateral resolution. Raman spectra were taken at each measurement point of the areas. Then raw data were evaluated by fitting the Raman bands with single or multiple Lorentzian curves representing band intensities, shifts or widths vs. position in the form of maps.

The laser-induced heating of SiGe islands can be rather strong, owing to a limited thermal drain[13,34]. In the case of SiGe islands studied here, the average heating effect on the Si-Si mode Raman shift was $\sim$ -2 $cm^{-1}mW^{-1}$ with our 0.95 N.A. lens. Therefore, we used the excitation power of $\sim$0.1 mW that makes downshift of only $\sim$0.2 cm^{-1} for the Si-Si band and even smaller one for the Ge-Ge and Si-Ge bands. This causes just a negligible error in the Ge content and strain determination.

Infrared (IR) transmittance spectra were measured using Shimadzu SolidSpec-3700 UV-visible-IR spectrophotometer.

III. RESULTS AND DISCUSSION

At first, we studied Raman spectra of UT-SGOI substrates before dewetting as a reference. Fig. 4 shows Raman spectra of three layered structures:
1) Si-rich 200 nm thick SiGe layer (Ge content x $\sim$ 0.3) deposited via molecular beam epitaxy on 14 nm thick UT-SOI (black curve);
2) Ge-rich 9 nm thick SiGe on 25 nm thick SiO2 (red curve) obtained from Ge condensation in the rapid thermal oxidation oven starting 21 nm SiGe layer (22% Ge content) deposited on 14 nm UT-SOI and condensed for 9 hours in the rapid thermal oxidation ovenat 750°C (see Fig. 1 for the corresponding TEM image).
3) 9.2 nm thick SiGe on 6 nm thick Si (blue curve) with approximately equal content of Si and Ge (see Fig. 1 for the corresponding TEM image).

The spectra display three bands originating from the Si-Si, Si-Ge and Ge-Ge bond vibrations. For Si-rich SiGe, the Si-Si mode Raman band is quite strong while the Ge-Ge mode band is very weak. In contrast to this, the Ge-Ge mode band is strong for the Ge-rich SiGe while the Si-Si mode band is very weak. All three bands display comparable intensities in the spectrum of the sample with approximately equal content

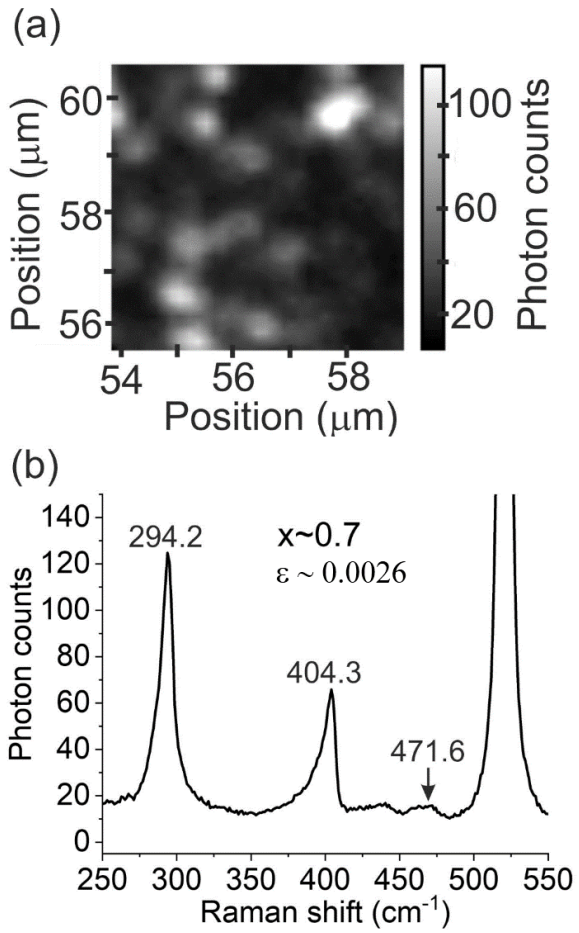

FIG. 6. (a) Raman intensity map of the Ge-Ge mode for the SiGe island sample fabricated from 9.2 nm thick SiGe layer as in Fig. 1 c). (b) Raman spectrum of a bright SiGe island; the Ge content x, determined from the Raman peak positions, is indicated.

of Si and Ge.

Dependencies of the frequencies of these modes ω(Si-Si), ω(Si-Ge) and ω(Ge-Ge) on the Ge content (x) and strain (ϵ) were studied in Refs.[35,36] Taking into account the results of these works and the values of the optical phonon frequencies in bulk Si ∼520.5 cm^{-1} and in bulk Ge ∼301.1 cm^{-1}, the SiGe mode frequencies satisfy the following equations:

$$\omega(Si-Si) = 520.5 - 66.9x - 730\epsilon \quad (1)$$

$$\omega(Si-Ge) = 401.1 + 24.5x - 4.5x^2 - 33.5x^3 - 70\epsilon \quad (2)$$

$$\omega(Ge-Ge) = 81.7 + 19.4x - 450\epsilon \quad (3)$$

For the Si-rich layer 1), we have found ω(Si-Si) ∼ 509.4 cm^{-1}, ω(Si-Ge) ∼ 407.4 cm^{-1} and ω(Ge-Ge) ∼ 301.5 cm^{-1}. For the Ge-rich layer, the frequencies were:

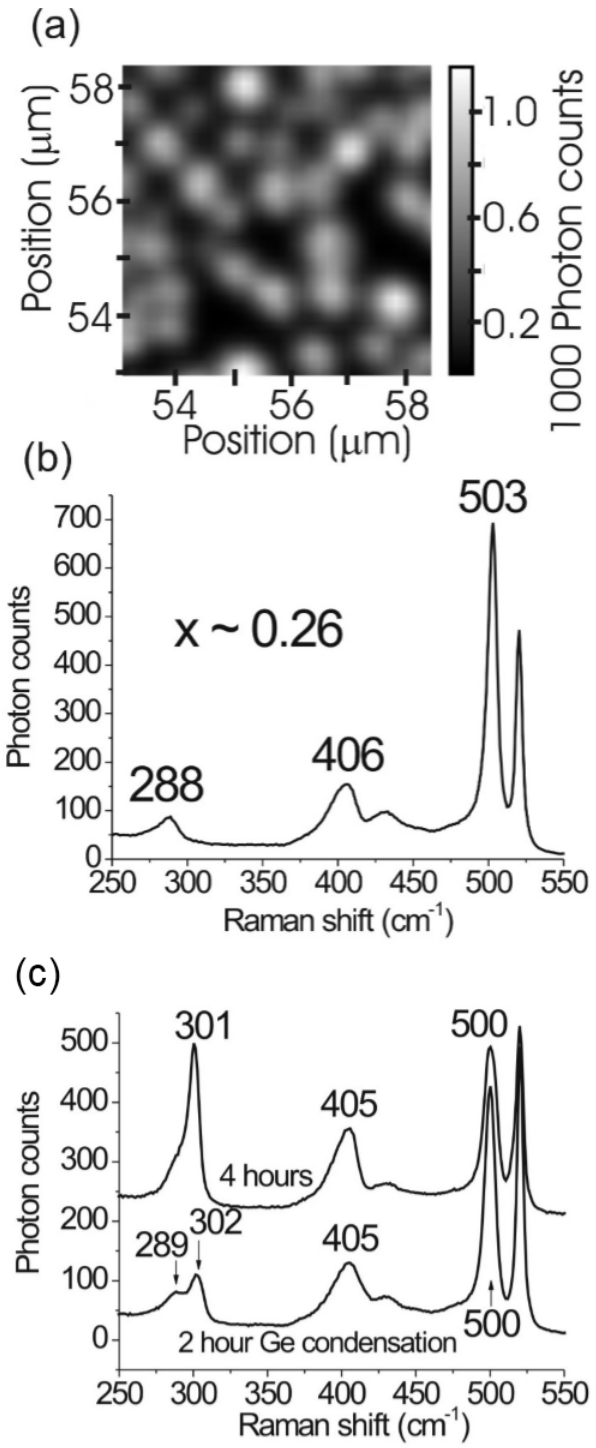

FIG. 7. (a) Raman intensity map of the Si-Si mode for the SiGe island sample fabricated from 50 nm thick SiGe layer (x ∼ 0.3) on 14 nm thick UT-SOI; (b) Raman spectrum of typical SiGe island; the Ge content x, determined from the Si-Si mode peak position, is indicated. (c) Raman spectra of typical SiGe islands as in (a) and (b), after 2 and 4 hours condensation in the rapid thermal oxidation oven (RTO).

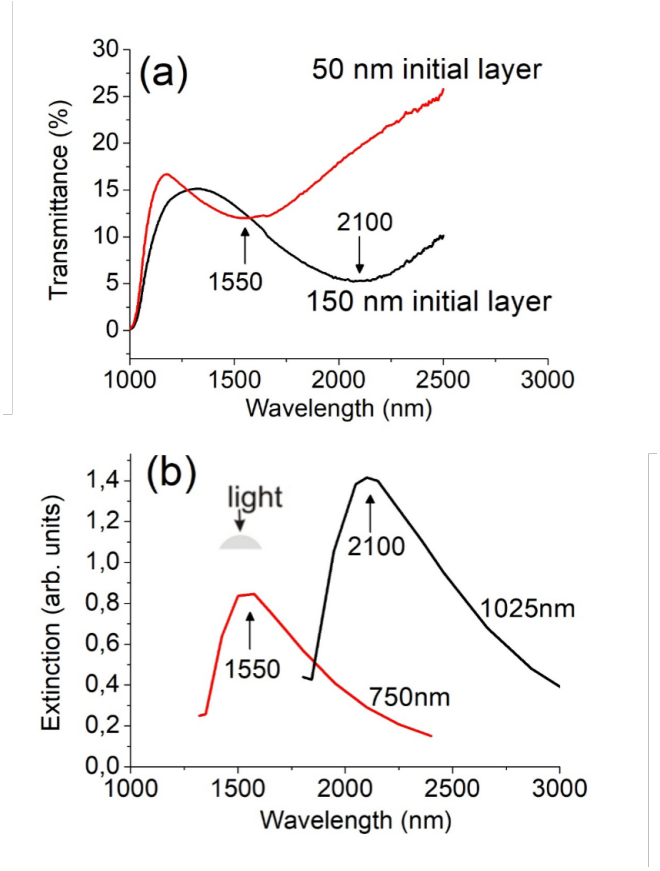

FIG. 8. (a) Experimental IR transmittance spectra of SiGe island arrays fabricated from 50 nm (red) and 150 nm (black) thick initial SiGe layers (x $\sim$ 0.3) on 14 nm thick UT-SOI; b) calculated extinction spectra of SiGe particles (x = 0.3) with the shape of segment of sphere (see the inset) with the aspect ratio of 0.23 and lateral sizes of 750 nm (red) and 1025 nm (black).

ω(Si-Si) $\sim$ 468 cm^{-1}, ω(Si-Ge) $\sim$ 407 cm^{-1} and ω(Ge-Ge) $\sim$ 304.5 cm^{-1}. For the third layer, we obtained ω(Si-Si) $\sim$ 502.2 cm^{-1}, ω(Si-Ge) $\sim$ 421.3 cm^{-1} and ω(Ge-Ge) $\sim$ 301.5 cm^{-1}.

Using experimentally determined SiGe mode frequencies and the equations (1), (2), (3), one can estimate x and ϵ as shown in Fig. 4. The Ge content appeared to be close to the expected one from the fabrication process[25–28]. The compressive strain in all three SiGe layers is quite strong up to ϵ $\sim$-0.027 for the partially condensed layer 3).

After dewetting and island formation from the condensed layer 3), the strain is very much relaxed. This can be seen in Fig. 5 displaying Si-Si band Raman intensity map and Raman spectra of two individual islands. The compressive strain ϵ $\sim$ -0.001 and -0.004 (close to the sensitivity of the measurement) is much smaller than ϵ $\sim$-0.027 measured in the initial SiGe layer. The Ge content in the islands x $\sim$0.35 and 0.46 is noticeably lower than $\sim$0.57 in the initial SiGe layer. This is an indication of mixing of SiGe with the 6 nm thick UT-SOI that was not yet consumed during the condensation process (see Fig. 1 b)).

For Ge-rich SiGe islands, we used the Ge-Ge mode band for Raman mapping. Its intensity map is shown in Fig. 6 a) together with a typical Raman spectrum of relatively bright islands (Fig. 6 b)). The Ge content x $\sim$ 0.7 is lower than $\sim$0.83 in the initial SiGe layer. Probably, Ge is partly substituted with Si from SiO_2. Strain is relaxed compared to ϵ $\sim$-0.015 in the initial SiGe layer.

Let us consider in more details Si-rich islands, which we used as a core for fabrication of Ge-rich shell (as shown in Fig. 3). Fig. 7 a) and b) respectively show Si-Si band Raman intensity map and corresponding spectrum of a SiGe islands obtained via 4 hour dewetting at $\sim$800°C from SiGe layers with x $\sim$ 0.3 and thicknesses 50 nm, on 14 nm thick UT-SOI substrate. Raman spectroscopy confirms a Ge content of about 30% and negligible strain. Qualitatively similar results were obtained for initial SiGe layer thickness of 80 and 150 nm (not shown).

The effect of Ge condensation after dewetting is clearly seen in the Raman spectra (Fig. 7 c)). Indeed, in addition to the Ge-Ge mode band at 288-289 cm^{-1}, one can see the band at 301-302 cm^{-1} indicating appearance of the pure Ge. For the sample obtained via two hour condensation, the Ge signal of the shell band at 302 cm^{-1} is rather weak and up-shifted compared to relaxed bulk Ge 301.1 cm^{-1} band suggesting a slight compression (ϵ $\sim$-0.002). With an increase in the condensation time up to four hours, the Ge band becomes stronger while strain is completely relaxed. This relaxation is understandable considering that the Si-rich core influence weakens while the Ge shell thickness increases.

Intensity maps of Si-Si and Ge-Ge modes from the same dewetted sample after 8 hour condensation show some islands brighter in the Si-Si mode map and others brighter in the Ge-Ge mode map (not shown). This can be interpreted as an indication of different shell thicknesses for islands having different initial size providing stronger Ge-Ge mode signal while suppressing the Si-Si mode signal. A possible origin of non-uniform shell thickness is the different initial Ge content in the dewetted islands. Provided that the condensation process selectively oxidizes Si, the speed at which it progresses is different depending on the initial Ge content of the island[16,25–28]: for larger Ge content the oxidation rate of Si is slower. Related to the same issue of non-uniform Ge content is the presence of strain that may, in principle, modify the atom diffusion in the underlying crystalline lattice.

Finally, we study SiGe particle IR spectra with Mie resonances. Fig. 8 a) shows IR transmittance spectra of two samples fabricated from 50 nm and 150 nm thick initial SiGe layers (x $\sim$ 0.3). The Raman maps for the 50 nm case was presented in Fig. 7a). The IR spectrum of the first sample displays transmittance minimum at $\sim$1550 nm while the spectrum of the second sample displays minimum at $\sim$2100 nm. The minima can be attributed to in-plane electric dipole Mie resonances in the SiGe islands with the shape of segment of sphere (as also confirmed by the TEM images of dewetted islands in Fig. 2 c))[13]. Low transmittance at 1000-1100 nm is associated with the Si substrate absorption. Longer wavelength of the Mie resonance of the second sample is justified

by the larger particle sizes as expected from the dewetting of thicker initial SiGe layers and confirmed by SEM microscopy (not shown): the lateral sizes of the particles in the first sample were in the range of 500-1000 nm whereas those in the second sample were in the range of 800-1500 nm.

Using discrete dipole approximation (ADDA code[37]), we made theoretical calculation of the extinction spectra of the SiGe particles (x = 0.3) with the shape of segment of sphere (see inset in Fig. 8 b)). Lateral sizes of the particles were 750 nm and 1025 nm with the aspect ratio (height to lateral size) of 0.23 close to those in Ref.[16]. Refractive index of the media was 1.0 while that of particles was 3.54 corresponding to the index of $Si_{0.7}Ge_{0.3}$ at $\sim$2 μm[38]. The resonance peak positions in good agreement with the experimental data suggesting that the average sizes of the particles are close to the chosen values of 750 nm and 1025 nm. The larger broadening of the experimental spectra with respect to the simulations can be interpreted as an effect of the rather large spread of particles size observed in experiments. We should note that this is just a rough estimation since we neglected SiGe refractive index dispersion and did not consider refractive index of the SiO_2 support layer and underlying Si substrate.

IV. CONCLUSION

To summarize, we fabricated SiGe islands with different Ge content using a variety of dewetting plus condensation techniques and studied their Raman spectra. Raman data were used for both Ge content and strain control. Relatively strong strain in the initial SiGe layers appeared to be completely relaxed in the SiGe islands after dewetting. Ge content in the islands is lower than that in the initial SiGe layers when x 0.5 while it remains nearly unchanged compared to the initial layers at x$\sim$ 0.3. Island size strongly depends on the initial SiGe layer thickness, other conditions being equal. Correspondingly, IR Mie resonances are displayed at longer wavelengths for larger islands fabricated from thicker initial SiGe layers.

V. ACKNOWLEDGMENTS

The authors are grateful to Dr. M. Yurkin for discussions and consultations regarding the ADDA code. The authors thank the Nanotecmat Platform of the IM2NP Institute of Marseille and the CP2M and CINaM microscopy centers of Aix-Marseille University. This work has received funding from Nano2017 FUI project, the European Union's Horizon 2020 research and innovation programme under Grant No. 654148 Laserlab-Europe. We also acknowledge the Projects PRCI network ULYSSES (No. ANR-15-CE24-0027-01) funded by the French ANR agency, the LASER-LAB Europe project ARES and the H2020 FET-OPEN project NARCISO (No. 828890) financed by the EU, the A*MIDEX Project (No. ANR-11-IDEX-0001-02) funded by the Investissements d'Avenir, a French Government program managed by the French National Research Agency (ANR).

[1] A. I. Kuznetsov, A. E. Miroshnichenko, M. L. Brongersma, Y. S. Kivshar, and B. Lukyanchuk, Science **354**, aag2472 (2016).
[2] I. Staude and J. Schilling, Nature Photonics **11**, 274 (2017).
[3] K. Baryshnikova, M. Petrov, V. Babicheva, and P. Belov, Scientific reports **6**, 22136 (2016).
[4] M. Garín, R. Fenollosa, R. Alcubilla, L. Shi, L. Marsal, and F. Meseguer, Nature communications **5**, 3440 (2014).
[5] R. Paniagua-Domínguez, Y. F. Yu, A. E. Miroshnichenko, L. A. Krivitsky, Y. H. Fu, V. Valuckas, L. Gonzaga, Y. T. Toh, A. Y. S. Kay, B. Lukyanchuk, *et al.*, Nature communications **7**, 10362 (2016).
[6] D. R. Abujetas, J. A. Sanchez-Gil, and J. J. Sáenz, Optics express **26**, 31523 (2018).
[7] A. B. Evlyukhin, C. Reinhardt, A. Seidel, B. S. Lukyanchuk, and B. N. Chichkov, Physical Review B **82**, 045404 (2010).
[8] Y. Kivshar and A. Miroshnichenko, Optics and Photonics News **28**, 24 (2017).
[9] R. M. Bakker, Y. F. Yu, R. Paniagua-Domínguez, B. Lukyanchuk, and A. I. Kuznetsov, Nano letters **17**, 3458 (2017).
[10] S. Kruk and Y. Kivshar, ACS Photonics **4**, 2638 (2017).
[11] M. Abbarchi, M. Naffouti, B. Vial, A. Benkouider, L. Lermusiaux, L. Favre, A. Ronda, S. Bidault, I. Berbezier, and N. Bonod, ACS Nano **8**, 11181 (2014).
[12] A. Shklyaev and A. Budazhapova, Applied Surface Science **360**, 1023 (2016).
[13] V. Poborchii, A. Shklyaev, L. Bolotov, N. Uchida, T. Tada, and Z. N. Utegulov, Applied Physics Express **10**, 125501 (2017).
[14] T. Wood, M. Naffouti, J. Berthelot, T. David, J.-B. Claude, L. Métayer, A. Delobbe, L. Favre, A. Ronda, I. Berbezier, *et al.*, ACS photonics **4**, 873 (2017).
[15] M. Naffouti, T. David, A. Benkouider, L. Favre, A. Ronda, I. Berbezier, S. Bidault, N. Bonod, and M. Abbarchi, Nanoscale **8**, 7768 (2016).
[16] M. Naffouti, T. David, A. Benkouider, L. Favre, M. Cabie, A. Ronda, I. Berbezier, and M. Abbarchi, Nanotechnology **27**, 305602 (2016).
[17] M. Bouabdellaoui, S. Checcucci, T. Wood, M. Naffouti, R. P. Sena, K. Liu, C. M. Ruiz, D. Duche, J. Le Rouzo, L. Escoubas, *et al.*, Physical Review Materials **2**, 035203 (2018).
[18] E. Bauer, Zeitschrift für Kristallographie-Crystalline Materials **110**, 372 (1958).
[19] M. Gurioli, Z. Wang, A. Rastelli, T. Kuroda, and S. Sanguinetti, Nature materials , 1 (2019).
[20] T. Coenen, J. van de Groep, and A. Polman, ACS nano **7**, 1689 (2013).
[21] E. Sutter and P. Sutter, Nanotechnology **17**, 3724 (2006).
[22] P. Zhang, B. Yang, P. Rugheimer, M. Roberts, D. Savage, F. Liu, and M. Lagally, Journal of Physics D: Applied Physics **42**, 175309 (2009).
[23] V. Poborchii, A. Shklyaev, L. Bolotov, and N. Uchida, Journal of Applied Physics **126**, 123102 (2019).
[24] E. Mitsai, M. Naffouti, T. David, M. Abbarchi, L. Hassayoun, D. Stozhenko, A. Mironenko, S. Bratskaya, S. Juodkazis, S. Makarov, and A. Kuchmizhak, Nanoscale (2019).

[25] T. David, A. Benkouider, J.-N. Aqua, M. Cabie, L. Favre, T. Neisius, M. Abbarchi, M. Naffouti, A. Ronda, K. Liu, *et al.*, The Journal of Physical Chemistry C **119**, 24606 (2015).
[26] T. David, K. Liu, S. Fernandez, M.-I. Richard, A. Ronda, L. Favre, M. Abbarchi, A. Benkouider, J.-N. Aqua, M. Peters, *et al.*, The Journal of Physical Chemistry C **120**, 20333 (2016).
[27] T. David, K. Liu, A. Ronda, L. Favre, M. Abbarchi, M. Gailhanou, P. Gentile, D. Buttard, V. Calvo, M. Amato, *et al.*, Nano letters **17**, 7299 (2017).
[28] T. David, J.-N. Aqua, K. Liu, L. Favre, A. Ronda, M. Abbarchi, J.-B. Claude, and I. Berbezier, Scientific reports **8**, 2891 (2018).
[29] V. Poborchii, T. Tada, and T. Kanayama, Applied physics letters **89**, 233505 (2006).
[30] V. Poborchii, T. Tada, and T. Kanayama, Applied Physics Letters **91**, 241902 (2007).
[31] V. Poborchii, T. Tada, and T. Kanayama, Applied Physics Letters **94**, 131907 (2009).
[32] V. Poborchii, T. Tada, Y. Morita, and T. Kanayama, Applied Physics Letters **103**, 153104 (2013).
[33] V. Poborchii, Y. Morita, M. Ishimaru, and T. Tada, Applied Physics Letters **105**, 153112 (2014).
[34] V. Poborchii, T. Tada, and T. Kanayama, Journal of applied physics **97**, 104323 (2005).
[35] F. Pezzoli, L. Martinelli, E. Grilli, M. Guzzi, S. Sanguinetti, M. Bollani, H. Chrastina, G. Isella, H. Von Känel, E. Wintersberger, *et al.*, Materials Science and Engineering: B **124**, 127 (2005).
[36] F. Pezzoli, E. Bonera, E. Grilli, M. Guzzi, S. Sanguinetti, D. Chrastina, G. Isella, H. Von Känel, E. Wintersberger, J. Stangl, *et al.*, Journal of applied physics **103**, 093521 (2008).
[37] M. A. Yurkin and A. G. Hoekstra, Journal of Quantitative Spectroscopy and Radiative Transfer **112**, 2234 (2011).
[38] P. Barritault, M. Brun, P. Labeye, O. Lartigue, J.-M. Hartmann, and S. Nicoletti, Optics express **21**, 11506 (2013).